Article

Stereochemistry of Transition Metal Complexes Controlled by the Metallo-Anomeric Effect

Feng Zhu and Maciej A. Walczak*

ACCESS | 📊 Metrics & More | 📰 Article Recommendations | 🆂🅸 Supporting Information

ABSTRACT: The use of stereoelectronic interactions to control reactivity and selectivity has a long history in chemistry. The anomeric effect, one of the fundamental concepts in organic chemistry, describes the preferences of a substituent at the anomeric carbon in glycosides to adopt axial configuration when the anomeric group is an electronegative element such as oxygen or a halogen. The origin of the anomeric effect has been the subject of intense debate. Explanations capitalizing on either the delocalization of the endocyclic oxygen lone pair into the antibonding $\sigma^*_{(C-X)}$ orbital or the minimization of the dipole−dipole interactions are currently the two leading theoretical models. Although the majority of experimental and theoretical studies have focused on the elements from groups 6 and 7, little is known about conformational preferences of tetrahydropyran rings substituted with a transition metal at the anomeric carbon and the role of these interactions in stereoselective synthesis. Here, we report studies on conformational and configurational preferences of organometallic complexes stabilized by vicinal heteroatoms. We provide computational evidence that late transition metals adopt the axial position in heterocycles or synclinal geometry in acyclic systems. Furthermore, the anomeric preferences of late transition metals correlate with the oxidation state of the metal and can be explained by hyperconjugative interactions between endocyclic heteroatom and the σ^* acceptor orbitals of the C−M bond. In a broader context, this discovery provides insight into the role of previously unanticipated stereoelectronic effects that can be harnessed in the design of stereoselective reactions, including chemical glycosylation and enantioselective catalysis.
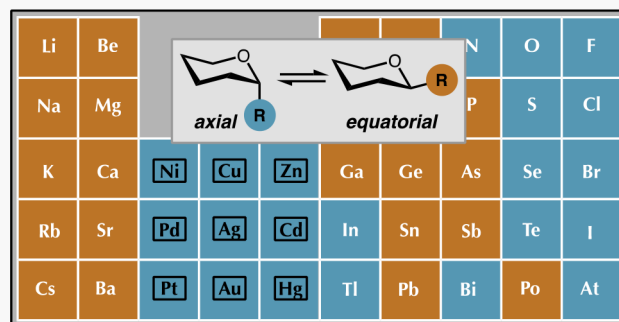
INTRODUCTION

Stereoelectronic control is one of the core concepts of modern organic chemistry.[1,2] In the realm of carbohydrates, the preference of a heteroatom substituent in a glycoside to adopt the axial position in a pyranose is termed as the anomeric effect (Scheme 1A).[3−8] Maximization of hyperconjugative[9,10] and minimization of electrostatic interactions[11] are often evoked as the major contributors to the increased stability of axial glycosides, which can be further reinforced by the exoanomeric effect dictating a maximal overlap between exocyclic oxygen lone pair with $\sigma^*_{(CO)}$ bond of the pyranose/furanose ring.[12] The opposite extreme is the destabilizing interaction of a positively charged substituent at C_1 such as a pyridinium ion that prefers the equatorial configuration (the reverse anomeric effect).[13,14] In more general terms, maximization of hyperconjugative interactions can be extended to acyclic systems (the gauche effect),[15] and it is often cited as the dominant factor responsible for the synclinal geometry of X−CH_2−CH_2−Y—type compounds.[16,17]

Unlike halogens and first-row main group elements, very little is known about configurational and conformational preferences of other elements located at the anomeric carbon. Particularly interesting are late transition metals relevant to modern catalytic cross-coupling reactions, and metals from groups 10, 11, and 12

have not been investigated in detail (Scheme 1B). A review of recent reactions involving the putative anomeric intermediates **3/4** indicates that transition metals may display strong preference toward the axial position, as judged by the preferential formation of axial products **6** (Scheme 1C). Cross-coupling reactions with anomeric bromides/chlorides and aryl organometallic reagents using Co,[18] Ni,[19−24] and Fe[25] catalysts indicate that the anomeric selectivities are dictated by anomeric preference of the transition metal center, provided that the C−C bond forming step occurs via a stereoretentive reductive elimination. Under photoredox/nickel dual catalytic conditions, C−C cross-couplings with Hantzsch esters **7** forming acyl and aryl *C*-glycosides **8** were reported.[23,24] These studies collectively suggest that high anomeric selectivities in these reactions demonstrate an inherent propensity of late transition metals to adopt the axial configuration.

Scheme 1. (A) An Overview of the Anomeric Effect; (B) Key Aspects of the Metallo-Anomeric Effect; (C) Selected Transition-Metal Catalyzed Coupling Reactions Proceeding via Anomeric Organometallic Intermediates (These Reactions Can Be Either Stereoretentive if Configurationally Stable Nucleophiles Are Used, Radical, or Cationic for Acetal Derivatives); and (D) Selected Cross-Coupling Reactions with Acyclic Systems Proceeding via Stabilized Radical Intermediates
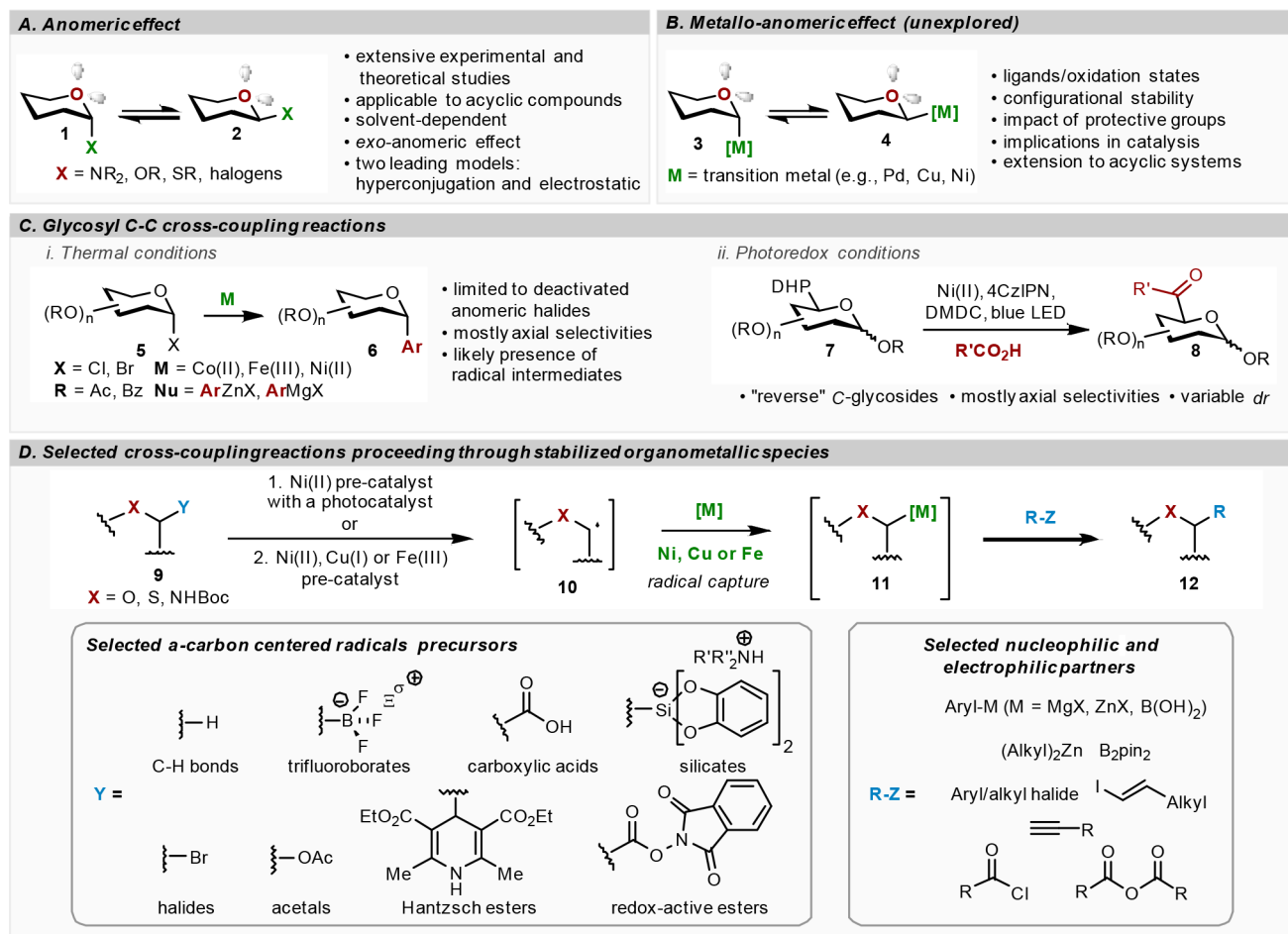
In addition to reactions with carbohydrate substrates, α-alkoxy, α-amino, and α-alkylthio heterocycles are structural motifs found in pharmaceutically relevant targets and substantial efforts have been devoted to developing methods for modification of the α position adjacent to a heteroatom (Scheme 1D). Metallaphotocatalysis represents a promising strategy due to the ease of formation of α-carbon-centered radicals, and multiple strategies for stabilized radical generation have been discovered.[26,27] An array of α-trifluoroborates could be cross-coupled with structurally diverse aryl and acyl electrophiles using the Ni/photoredox dual catalysis.[28−34] Alkyl bis(catecholato)silicates are latent α-carbon radicals precursors and were engaged in $C(sp^3)−C(sp^2)$ metallaphotoredox cross-couplings with aryl or vinyl halides.[35−37] Carboxylic acids as an alternative to these methods have also proven efficient in decarboxylative $C(sp^3)−C(sp^2)$ cross-coupling of α-amino- and α-oxycarboxylic acids.[38−43] Recent reports also demonstrate that 1,4-dihydropyridines,[23,24,44] α-alkoxymethyl halides,[45] and benzylic acetals[45] can provide access to α-carbon-centered radicals. A combination of photoredox and nickel catalysis was proven effective in arylation or alkylation of α-amino-, α-oxy-, and α-thio-$C(sp^3)$−H bonds in both cyclic and acyclic systems.[46−54] To complement these studies, redox-active esters were developed,[55] and Ni- or Fe-catalyzed cross-couplings with suitable nucleophilic reagents resulting in a series of

arylation or alkylation products of α-amino, α-oxy cyclic, and acyclic carboxylic acid,[56−59] as well as decarboxylative borylation catalyzed by Cu(I) or Ni(II) were achieved.[60,61] In all of these cases, putative α-heteroatom-stabilized intermediates **11** were postulated, yet their structural analyses remain elusive.

Intrigued by the apparent lack of a comprehensive analysis of conformational preferences of α-alkoxyorganometallic complexes, we undertook a systematic study featuring a three-pronged approach focused on (a) computational analysis of conformational preferences of late transition metals bound to the α-carbon in tetrahydropyran, (b) analysis of monosaccharides and saturated heterocycles, and (c) analysis of conformational preferences of acyclic systems. These studies combined led us to propose that *late transition metals located at the anomeric carbon display strong axial preference (termed here as the metallo-anomeric effect)*, and this observation can rationalize anomeric selectivities in C−C and C-heteroatom bond-forming reactions. In cases where significant steric interactions can perturb the electronic stabilization, delocalization from vicinal heteroatom reinforces the axial structure when compared to the cyclohexane counterparts.

■ RESULTS AND DISCUSSION

In order to shed light on stereoelectronic effects in transition metal complexes and place experimental observations in a

1	2	10	11	12	13	14	15	16	17
Li Li −4.80 (−4.69) −5.90 (−5.60)	**Be** BeCl −0.96 (−1.23) −1.46 (−1.73)		reaction scheme 13 ⇌ 14 $\Delta E(O) = E_{eq}(O) - E_{ax}(O)$ Eq. (1); $AE = \Delta E(O) - \Delta E(CH_2)$ Eq. (2); Element / R group / $E_{eq}(O)-E_{ax}(O)$ / AE		**B** B(OMe)$_2$ −0.46 (−1.24) −0.73 (−0.30)	**C** CMe$_3$ −6.00 (−6.91) −1.34 (−0.39)	**N** NMe$_2$ 1.01 (0.66) 0.86 (0.51)	**O** OMe 1.33 (1.35) 1.38 (1.80)	**F** F 2.47 (2.29) 2.59 (2.51)
Na Na −3.80 (−3.34) −5.46 (−4.71)	**Mg** MgCl −6.13 (−5.85) −7.53 (−7.45)				**Al** Al(OMe)$_2$ −4.55 (−4.17) −5.82 (−5.22)	**Si** SiMe$_3$ −3.16 (−5.25) −1.19 (−1.85)	**P** PMe$_2$ −1.06 (−1.38) 1.42 (2.97)	**S** SMe 1.04 (0.48) 1.65 (0.89)	**Cl** Cl 3.29 (2.91) 3.52 (3.30)
K K −3.40 (−3.56) −5.17 (−3.81)	**Ca** CaCl −6.04 (−5.62) −0.71 (−2.97)	**Ni** NiClPhen 0.41 (0.64) 2.83 (3.25)	**Cu** Cu 3.13 (2.29) 1.75 (0.77)	**Zn** ZnCl 0.92 (1.78) −0.25 (0.95)	**Ga** GaMe$_2$ 0.07 (−1.07) −1.32 (−4.12)	**Ge** GeMe$_3$ −2.26 (−4.44) −0.94 (−1.91)	**As** AsMe$_2$ −0.81 (1.26) 0.15 (2.22)	**Se** SeMe 1.60 (1.66) 2.23 (2.11)	**Br** Br 4.16 (3.79) 4.33 (4.14)
Rb Rb −3.05 (−3.05) −2.61 (−1.77)	**Sr** SrCl −5.34 (−5.90) −3.58 (−5.50)	**Pd** PdClPhen 3.02 (3.25) 4.86 (5.73)	**Ag** Ag 4.01 (4.23) 2.43 (1.94)	**Cd** CdCl 1.61 (1.21) 0.31 (−0.10)	**In** InMe$_2$ 0.13 (0.12) −1.65 (0.17)	**Sn** SnMe$_3$ −1.04 (−4.34) −0.85 (−2.83)	**Sb** SbMe$_2$ −0.96 (−3.58) −0.32 (−2.87)	**Te** TeMe 1.59 (1.56) 2.07 (1.95)	**I** I 4.54 (4.06) 4.70 (4.46)
Cs Cs −3.10 (−3.66) −4.91 (−5.10)	**Ba** BaCl −4.53 (−5.70) −0.72 (−2.98)	**Pt** PtClPhen 2.50 (2.20) 4.18 (4.84)	**Au** Au 4.73 (4.23) 3.88 (3.17)	**Hg** HgCl 1.88 (1.53) 0.94 (1.01)	**Tl** TlMe$_2$ −0.87 (1.18) −0.70 (−0.74)	**Pb** PbMe$_3$ 0.46 (−1.09) 0.12 (−1.12)	**Bi** BiMe$_2$ −0.91 (0.15) −0.54 (2.23)	**Po** PoMe 1.86 (−3.30) 2.23 (−3.07)	**At** At 4.81 (4.38) 4.92 (4.72)

Figure 1. Conformational analysis of substituted tetrahydropyran derivatives of selected elements in a chair conformation. All compounds calculated at M06-2X/def2QZVP//M06-2X/def2TZVP and refer to the lowest energy conformer for the axial and equatorial isomers. $\Delta E(O)$ refers to the difference of electronic energies between equatorial and axial isomers in a substituted tetrahydropyran in a chair form (Gibbs free energies at 298 K reported in parentheses). $\Delta E(CH_2)$ refers to the difference of electronic energies between equatorial and axial isomers in a substituted cyclohexane in a chair form (Gibbs free energies at 298 K reported in parentheses). AE refers to the difference of electronic energies and Gibbs energies at 298 K (in parentheses). Background coding: orange/blue = equatorial/axial isomer preferred. Phen = 1,10-phenanthroline, Me = methyl.

Table 1. Analysis of Substituted Tetrahydropyran Derivatives and Hyperconjugative Interactions between $n_{(O)}$ and $\sigma^*_{(CM)}/\sigma^*_{(CH)}$ [a]
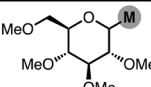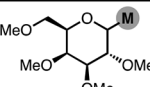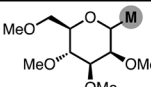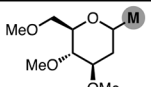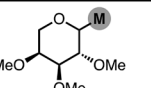
Entry	Metal	$E_{eq} - E_{ax}$ [kcal·mol^{-1}]	AE [kcal·mol^{-1}]	$d_{ax} - d_{eq}$ [Å]	Entry	Metal	$E_{eq} - E_{ax}$ [kcal·mol^{-1}]	AE [kcal·mol^{-1}]	$d_{ax} - d_{eq}$ [Å]
		Group 10			17	Cu(PMe$_3$)$_3$	−1.18 (−1.15)	−2.64 (−1.52)	−0.004
1	Ni	2.67 (2.57)	1.03 (0.85)	0.047	18	CuIm	0.03 (−0.46)	−1.19 (−0.93)	0.011
2	NiCl(PH$_3$)$_2$	−1.66 (−2.91)	−0.39 (−1.01)	0.021	19	CuClPMe$_3$	5.90 (5.06)	4.30 (2.84)	0.177
3	NiCl(NH$_3$)$_2$	−1.82 (−3.20)	−0.90 (−0.58)	0.025	20	CuClPhen	−0.43 (−0.19)	0.28 (0.50)	0.042
4	NiCl(PMe$_3$)$_2$	−2.60 (−4.20)	−0.53 (0.36)	0.019	21	CuCl$_2^-$	4.82 (5.12)	4.94 (3.67)	0.826
5	Pd	2.77 (2.34)	2.08 (1.61)	0.021	22	AgIm	1.00 (2.60)	−0.53 (1.26)	0.024
6	PdCl(PH$_3$)$_2$	−0.16 (−1.75)	1.57 (1.13)	0.027	23	AgClPMe$_3$	4.92 (2.64)	3.41 (1.87)	−0.149
7	PdCl(NH$_3$)$_2$	−0.06 (−1.86)	0.60 (0.84)	0.024	24	AuPMe$_3$	0.86 (0.55)	0.06 (0.54)	0.017
8	PdCl(PMe$_3$)$_2$	−1.46 (−3.27)	1.82 (1.37)	0.023	25	AuIm	0.57 (0.16)	−0.35 (−0.28)	0.016
9	cis-PdCl(PMe$_3$)$_2$	−1.65 (−2.17)	4.99 (5.78)	0.038	26	AuClPMe$_3$	12.1 (12.3)	12.0 (11.4)	1.010
10	PdCldmpe	−0.87 (−2.01)	3.68 (3.23)	0.041	27	AuCl$_2$PMe$_3$	1.18 (1.67)	5.03 (6.14)	0.076
11	PtCl(PH$_3$)$_2$	1.87 (0.24)	4.48 (2.85)	0.028			**Group 12**		
12	PtCl(NH$_3$)$_2$	−0.59 (−1.67)	−0.14 (1.06)	0.017	28	ZnF	0.87 (0.67)	−0.20 (−0.47)	0.032
13	PtCl(PMe$_3$)$_2$	−3.14 (−4.75)	0.71 (−2.87)	0.023	29	ZnBr	0.91 (0.83)	−0.29 (−0.17)	0.033
		Group 11			30	CdF	1.54 (1.56)	0.28 (0.31)	0.040
14	CuPy	0.74 (0.51)	−0.33 (−0.37)	0.021	31	CdBr	1.63 (1.35)	1.32 (1.29)	0.043
15	CuPMe$_3$	0.58 (−2.01)	−0.63 (−3.50)	0.021	32	HgF	1.74 (0.04)	0.92 (0.85)	0.034
16	Cu(PMe$_3$)$_2$	−0.10 (−0.35)	−2.64 (−1.51)	0.012	33	HgBr	1.97 (0.04)	1.01 (1.06)	0.038

[a] $E_{eq} - E_{ax}$ and AE defined as in Figure 1 and calculated at M06-2X/def2QZVP//M06-2X/def2TZVP level of theory. $d_{ax}-d_{eq}$ refers to the difference between C-M bond lengths in axial and equatorial isomers. dmpe = 1,2-bis(dimethylphosphaneyl)ethane; Im = 1,3-dimethyl-1,3-dihydro-2λ^2-imidazole; Py = pyridine. Background coding: orange/blue = equatorial/axial isomer preferred; green/purple = positive/negative AE values.

theoretical context, we conducted studies covering main group elements (groups 1−2 and 13−17) and transition metal complexes from groups 10−12. A truncated periodic table shown in Figure 1 was used as a guide to benchmark the preferences of these compounds. A uniform computational scheme representing a compromise between accuracy and effort was set up to evaluate various substituents in tetrahydropyran systems **13** and **14** locked in a chair conformation. To understand the sign and magnitude of anomeric stabilization, this study involved analysis of the corresponding cyclohexane derivatives, and the energy of the anomeric effect (AE) was calculated by the reaction scheme shown in eq 2 (Figure 1). As some compounds exist in multiple stable conformers resulting from rotation at the anomeric carbon and the side chains, only the most stable isomer for each tetrahydropyran epimer was

Table 2. Analysis of Axial and Equatorial Isomers of Selected Monosaccharides as Chair Conformers[a]

Metal	D-glucose	D-galactose	D-mannose	2-deoxy-D-glucose	D-arabinose
Group 10					
NiCl(PMe₃)₂	−7.12 (−8.59)	−8.75 (−8.40)	−1.19 (−1.11)	−2.13 (−3.50)	−6.89 (−7.16)
PdCl(PMe₃)₂	−10.3 (−9.56)	−5.60 (−7.72)	−2.20 (−3.31)	−0.34 (−2.39)	−5.67 (−5.66)
PtCl(PMe₃)₂	−8.47 (−10.7)	−11.0 (−12.1)	−3.66 (−4.09)	−1.85 (−3.88)	−7.90 (−8.21)
Group 11					
Cu	2.86 (2.38)	2.60 (2.15)	1.31 (0.66)	2.75 (2.61)	3.03 (2.50)
Ag	3.22 (3.07)	3.29 (2.65)	1.97 (1.46)	3.34 (3.09)	3.70 (3.25)
Au	3.14 (2.27)	3.79 (2.48)	4.39 (4.16)	4.39 (4.07)	4.13 (4.32)
Group 12					
ZnF	1.90 (2.09)	1.24 (1.78)	−4.15 (−3.99)	0.34 (0.35)	2.44 (2.21)
CdF	2.27 (2.38)	1.86 (1.69)	−2.60 (−2.71)	1.00 (1.00)	2.57 (1.29)
HgF	1.58 (1.14)	1.56 (1.37)	−0.54 (−1.07)	1.26 (1.14)	1.95 (1.87)

[a]For all compounds, the lowest energy axial and equatorial isomers were used. Background coding: orange/blue = equatorial/axial isomer preferred.

used to derive conclusions regarding the thermodynamic stabilities.

The calculated trends for alkaline and alkaline earth metals indicate a strong equatorial preference (ΔG° = −3.05 to −4.69 kcal·mol^{-1}) for these compounds. These results are consistent with the experimentally determined stabilities of C1-organo-lithium reagents,[62−64] and the equatorial bias in group 1 decreases as the size of the metal increases moving down the group. In this case, the anomeric effect energy is strongly negative (ΔG° = −1.77 to −5.60 kcal·mol^{-1}) as one would expect from the analysis of the equatorial preferences in the tetrahydrofuran derivatives. Organolithium compounds are likely to exist in solution as multimeric aggregates stabilized by a solvent, therefore the reverse anomeric effect is expected to be higher under condensed-phased conditions than the calculated values. Along similar lines, group 2 metals show very strong propensity to adopt the equatorial position irrespective of the size of the metal and the length of the ionic bond at the anomeric carbon. At the other end of the periodic table, halogens and chalcogens show strong bias toward the axial orientation with the calculated ΔG° values corresponding to the experimentally determined values in monosaccharides. Moving to group 13 and 14, equatorial isomers are favored, but in the case of the representative In(III) and Tl(III) structures, the axial isomers are slightly favored, likely due to elongation of the C−M bonds. Group 13 and 14 compounds show, expectedly, negative AE values. Group 10, 11, and 12 complexes in Figure 1 display strong thermodynamic propensity toward axial isomers. This trend is retained for group 10 square planar complexes of Ni(II), Pd(II), and Pt(II) stabilized by 1,10-phenanthroline, and group 11 and 12 organometallics in a d^{10} configuration. Remarkably, the anomeric stabilization in these three groups is comparable to halogens (ΔG° = 2.51−4.72 kcal·mol^{-1}), and in the series of Ni, Pd, and Pt, the metallo-anomeric effect energies AE range from ΔG° = 3.25 to 5.73 kcal·mol^{-1}.

Intrigued by these observations, we next performed a systematic analysis to understand the influence of metal configuration, spin, and oxidation state, and ligands attached directly to the metal on the stereochemistry of tetrahydropyran complexes **15** and **16** (Table 1). Nickel(I) and palladium(I) compounds (entries 1 and 5) show strong axial preferences and noticeable anomeric stabilizations (AE = 0.85 and 1.61 kcal·mol^{-1}, respectively). However, when phosphine or amine ligands are added to Ni(II) or Pd(II) forming 14-electron complexes (entries 2−4 and 6−10), the thermodynamic
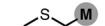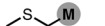
preferences revert to the equatorial isomers. This change is likely caused by the steric bulk of the ligands, and the increase in equatorial preferences moving from a small phosphine (PH₃) to PMe₃ is indicative of the critical impact of this component, even though these complexes remain coordinatively unsaturated. A less stable cis-configured Pd(II) complex (entry 9) shows a marked decrease of the equatorial preference as the steric clash between the phosphines and tetrahydropyran can be minimized by rotating the phosphines away from the ring. Similarly, a bidentate ligand is an excellent example of minimization of steric interactions caused by rearranging the ligands at the metal center (entry 10). Group 10 metals, in general, show high AE stabilization energies except for Ni(II), where a small ligand has little impact on stabilizing the equatorial isomer in cyclohexane (entries 2 and 3). It is interesting to note that the extent of the metallo-anomeric effect is comparable or can surpass classical examples of the anomeric effect as halogens (see Figure 1).

Moving to group 11, copper(I) structures prefer the axial configuration, but when ligands such as phosphine or amine are located in the linear configuration, they counteract the effect of the vicinal delocalization from endocyclic oxygen atom (entry 14 and 15). The thermodynamic preferences can be also influenced by the size and the number of ligands directly attached to the metal, and Cu(I) 16- and 18-electron complexes (entry 16 and 17) are illustrative of the critical impact of the number and electron count on the axial stabilization.

Silver and gold follow the metallo-anomeric effect and prefer the axial configuration (entries 22−27). Consequently, even strongly donating ligands such as N-heterocyclic carbenes (NHCs) are unable to override the inherent preferences of the metal in this series. Gold exclusively prefers axial anomers, and the magnitude of anomeric stabilization is dependent on the formal oxidation state of the metal and the total number of electrons (entries 24−27). For example, axial Au(II) structure as a 14-electron complex (entry 26) is significantly more stable than Au(III) with 16 electrons (entry 27).
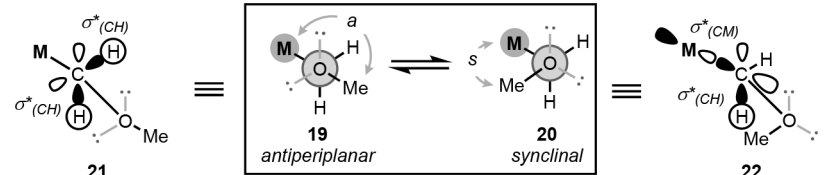
In group 12, linear complexes of Zn(II), Cd(II), and Hg(II) show consistently high axial preferences regardless of the nature of a halogen atom attached (entries 28−33). Zinc in this category stands out as the AE stabilization is reversed due to increased stability of the axial zinc cyclohexane structures over the corresponding equatorial isomers. The calculated axial stabilizations of Hg(II) in tetrahydropyran and cyclohexane are consistent with the experimental A values for Hg(II) salts.[65]

Table 3. Thermodynamic Properties of Group 10, 11, and 12 Heterocyclic Complexes[a]

Entry	Metal	$E_{eq} - E_{ax}$ [kcal·mol^{-1}]	AE [kcal·mol^{-1}]	$E_{eq} - E_{ax}$ [kcal·mol^{-1}]	AE [kcal·mol^{-1}]	$E_{eq} - E_{ax}$ [kcal·mol^{-1}]	AE [kcal·mol^{-1}]
Group 10							
1	NiCl(PMe$_3$)$_2$	−11.8 (−12.1)	−9.74 (−7.54)	−3.42 (−5.20)	−1.40 (−3.10)	−6.42 (−7.78)	−4.37 (−5.72)
2	PdCl(PMe$_3$)$_2$	−5.23 (−6.28)	−1.95 (−1.64)	0.21 (−1.67)	3.49 (1.61)	−5.97 (−8.06)	−2.69 (−4.78)
3	PtCl(PMe$_3$)$_2$	−6.60 (−7.93)	−2.75 (−5.72)	−1.48 (−3.51)	2.37 (0.34)	−7.50 (−9.56)	−3.65 (−5.71)
Group 11							
4	Cu	1.10 (0.85)	−0.28 (−0.67)	3.55 (2.99)	2.17 (1.61)	0.04 (−0.40)	−1.34 (−1.78)
5	Ag	1.61 (1.31)	0.04 (−0.30)	4.88 (4.21)	3.31 (2.64)	0.62 (0.10)	−0.95 (−1.47)
6	Au	2.97 (2.58)	2.12 (1.52)	7.03 (6.33)	6.18 (5.48)	3.54 (2.96)	2.69 (2.11)
Group 12							
7	ZnF	0.84 (0.78)	−0.23 (−0.36)	0.31 (0.12)	−0.80 (−0.90)	0.00 (0.00)	−1.07 (−1.07)
8	CdF	0.95 (0.85)	−0.30 (−0.40)	1.26 (0.96)	0.01 (−0.30)	0.10 (0.72)	−1.15 (−1.32)
9	HgF	1.33 (1.11)	0.51 (0.68)	1.90 (1.53)	1.08 (0.71)	1.19 (0.85)	0.37 (0.03)

[a]Background coding: orange/blue = equatorial/axial isomer preferred; green/purple = positive/negative AE values.

Table 4. Conformational Analysis of Methoxymethane Complexes with Group 10 and 11 Organometallic Complexes Calculated at M06-2X/def2QZVPP Level of Theory[a]

entry	metal	$E_a - E_s$ (kcal·mol^{-1})	θ_s	$d_s - d_a$ (Å)	$\mu_s - \mu_a$ (D)	entry	metal	$E_a - E_s$ (kcal·mol^{-1})	θ_s	$d_s - d_a$ (Å)	$\mu_s - \mu_a$ (D)
1	Ni	1.40 (1.00)	59.5	0.035	0.40	10	CuF	9.57 (12.0)	90.3	0.037	4.28
2	Pd	2.96 (2.35)	74.4	0.009	0.60	11	CuClPhen	5.97 (6.08)	63.9	0.021	−1.36
3	NiCl(PMe$_3$)$_2$	0.28 (−0.65)	65.6	−0.006	−0.93	12	CuCl$_2$	3.76 (4.18)	68.6	0.023	−0.81
4	PdCl(PMe$_3$)$_2$	1.83 (1.01)	68.3	0.012	−0.88	13	AgPMe$_3$	0.18 (0.37)	62.6	0.020	0.79
5	PtCl(PMe$_3$)$_2$	1.43 (5.81)	69.2	0.011	−1.00	14	AgIm	−0.14 (−1.59)	62.0	0.019	0.91
6	PtCl$_5^-$	7.81 (5.81)	77.7	0.030	−0.56	15	AuPMe$_3$	0.15 (−2.23)	65.6	0.012	0.98
7	CuPMe$_3$	−0.53 (−0.57)	61.3	0.017	0.87	16	AuIm	−0.14 (0.32)	65.5	0.011	1.05
8	CuIm	−0.95 (−1.23)	63.2	0.019	1.14	17	AuCl$_2^-$	6.70 (5.78)	69.2	0.075	−0.44
9	CuCl	18.6 (20.2)	84.3	0.114	5.22	18	AuCl$_2$PMe$_3$	3.94 (2.83)	78.1	0.048	0.33

[a]Antiperiplanar (a) and synclinal (s) conformers defined in **19** and **20**. Two hyperconjugative interactions between $n_{(O)}$ and $\sigma^*_{(CM)}/\sigma^*_{(CH)}$ shown in **21** and **22** control the conformational preferences, and the energy difference between the two antibonding orbitals is the dominant contribution. $E_a - E_s$ defined as electronic energy difference between the antiperiplanar and synclinal conformers (Gibbs free energy differences at 298 K in parentheses). Dihedral angle of the lowest energy synclinal conformer defined as θ_s. The difference between total dipole moments of the most stable synclinal and antiperiplanar isomers defined as $\mu_s - \mu_a$.

Several general trends regarding the nature of the metallo-anomeric effect can be derived from Table 1:

(A) Axial stabilization increases as the oxidation state of the metal increases, and complexes of Cu and Au are a good example of this trend. For Pd(IV) structures that were recently postulated as reactive intermediates in a C−H activation/C-glycosylation of mannose, the high anomeric selectivities are consistent with the nature metallo-effect and the effect of high oxidation state (for details, see the Supporting Information, SI).[66]

(B) Moving from a lighter to a heavier element within the same group, the axial preferences increase. This phenomenon can be attributed to a change in electronegativity and atomic radius/bond elongation resulting in increased σ-acceptor properties of the C−M bonds.[67] Group 11 and gold complexes, in particular, are a good example of this feature, and their axial preferences are retained in every structure studied here regardless of the ligand attached. Both, the absolute value and the magnitude of the anomeric effect measured by AE values

increase within each group moving from a lighter to a heavier element.

(C) Axial complexes have longer C−M bonds and the extent of C−M bond elongation is dependent on the oxidation state of the metal (e.g., entry 21).

(D) Strongly electron-donating ligands such as *N*-heterocyclic carbenes can counteract the metallo-anomeric effect, and complexes with higher electron count favor the axial isomer to a lesser extent. This situation originates from a change in electron density at the metal as well as increased steric bulk.

Subsequent studies on the metallo-anomeric effect focused on conformational analysis of group 10, 11, and 12 metals located at the anomeric position in common monosaccharides (Table 2). C1-Organopalladium intermediates were proposed in cross-couplings with anomeric nucleophiles[63] and directed *C*-arylation,[66] therefore their thermodynamic behavior is relevant to the observed axial selectivities. The overall trend in pyranose monosaccharides parallels the preferences in tetrahydropyran derivatives except for group 12 metals in the mannose series in which the equatorial isomers are more stable because of
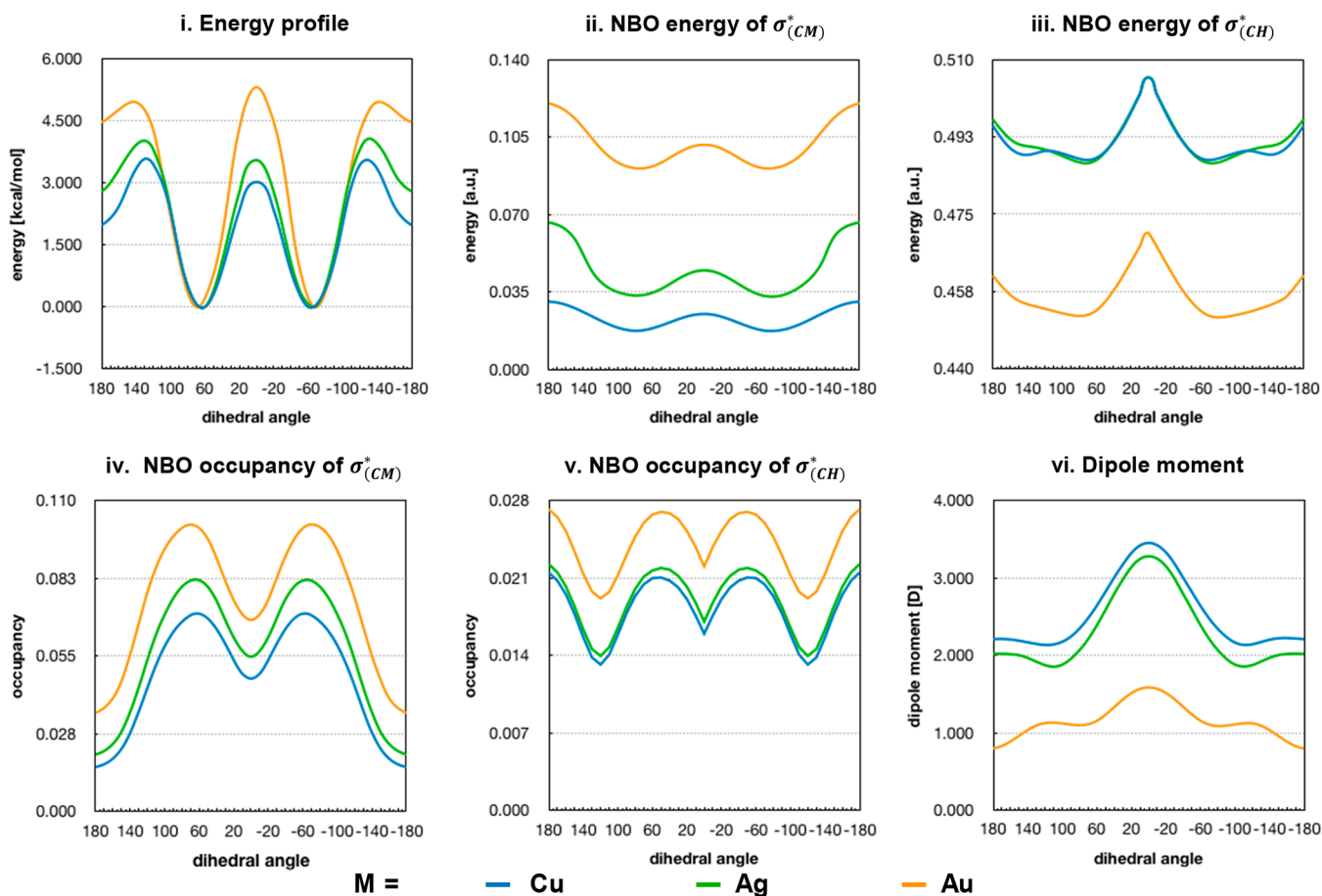
Figure 2. Conformational analysis of Cu, Ag, and Au complexes. Changes in electronic energy calculated at M06-2X/def2QZVPP level of theory. NBO analyses performed at the same level of theory and refer to $\sigma^*_{(CM)}$ and $\sigma^*_{(CH)}$ shown in **21/22**. For all calculations, dihedral angle defined as M−C−O−$C_{(Me)}$.

coordination of the C2 group with the electrophilic metal centers. Arabinose and 2-deoxyglucose structures were also analyzed to understand the electronic effect of oxygen substitution within the established armed−disarmed framework. Many 2-deoxy-glucose derivatives show increased propensity to adopt the axial configuration when in a chair conformation because of a reduced steric clash between the C2 substituent and the ligands at the metal center.

In the arabinose series, the same trend becomes apparent when compared to galactose that has an analogous configuration but possesses an additional carbon side chain.

Because the nature and the number of the stabilizing heteroatom may impact the magnitude of the metallo-anomeric effect, conformational analysis was performed on substituted 1,3-dioxanes, tetrahydro-2H-thiopyrans, and 1,3-dithianes (Table 3). The stereochemical preferences of anions derived from these parent compounds are well-established.[68] Replacing the oxygen atom in tetrahydropyran with sulfur results in a decrease of axial preference by $\Delta\Delta G°$ 2.3 kcal mol^{-1} on average, and general conformational trend across all studied systems parallels the behavior of tetrahydropyran. Additional vicinal oxygen atom in 1,3-dioxane increases the axial preference in group 11 elements but can skew the preferences in group 10 and 12 metals in either direction. Two sulfur atoms in 1,3-dithianes have less pronounced effect on the axial orientation. Interestingly, across all three heterocycles, only the heaviest

elements in group 11 and 12 series (Au(I) and Hg(I)) show positive AE values.

Next, studies on the conformational features of heteroatom-substituted organometallic complexes were applied to acyclic systems (Table 4). A survey of substituents based on group 10 and group 11 derivatives revealed that the synclinal conformers are preferred over the antiperiplanar isomers irrespective of the configuration at the transition metal and ligands attached. This trend is reminiscent of the generalized anomeric effect that is governed by the maximization of hyperconjugative interactions between $n_{(O)}$ and $\sigma^*_{(CO)}$ bonds.[69] One notable exception in this series are NHC complexes (entry 8, 14, and 16), which, similarly to the tetrahydropyran systems, prefer the antiperiplanar orientation. Conformational preferences of Ni, Pd, and Pt complexes stand in contrast to structures of these of tetrahydropyran and 1,3-dioxane systems, providing direct evidence that high equatorial preferences are a consequence of steric clash between the ligands on the metal and methylene groups in tetrahydropyran and analogs.

To better understand the nature of the metallo-anomeric effect, we performed Natural Bond Orbital (NBO) analysis,[70] and Figure 2 depicts a detailed conformational analysis of Cu(I), Ag(I), and Au(I) complexes. The NBO formalism allows for a quantitative assessment of stereoelectronic effects, and the stabilization energy E_2 associated with delocalization of electrons in idealized Lewis structures into the empty non-Lewis orbitals was successfully applied to analyze the classical

anomeric effect.[9,71] Several general trends can be derived from these studies:

(A) Delocalization of heteroatom nonbonding electrons into $\sigma^*_{(CM)}$ is the dominant factor controlling the axial/equatorial and synclinal/antiperiplanar preferences of late transition-metal complexes. In cases where the sterics overrides the electronic component (e.g., group 10 examples), the energetic gains from mixing of $n_{(O)}$ electrons and antibonding orbitals are still substantial. Several lines of evidence support the hypothesis that electron delocalization is the main component responsible for axial stability of transition metal complexes—the E_2 values of $n_{(O)} \rightarrow \sigma^*_{(CM)}$ delocalizations for all axial structures for group 10, 11, and 12 from Figure 1 show highly stabilizing interactions with the nonbonding electrons (6.2−25.2 kcal·mol⁻¹), which are comparable to the analogous axial delocalizations in 2-halotetrahydropyran (23.1, 25.1, and 29.9 kcal·mol⁻¹ for F, Cl, and Br, respectively; values calculated at M06-2X/def2QZVP level of theory for all series).

(B) As the metal undergoes rotation around the single bond in **19/20**, the energy of $\sigma^*_{(CM)}$ changes in response to mixing with nonbonding orbitals from the heteroatom and reaches the lowest point in the synclinal stereoisomer (Figure 2-ii). Along the same lines, the occupancy of $\sigma^*_{(CM)}$ increases by approximately 300%−450% in the synclinal conformer **20** when compared to the antiperiplanar structures **19**, which have the lowest $\sigma^*_{(CM)}$ populations (Figure 2-iv). The antibonding orbitals $\sigma^*_{(CH)}$, alternative acceptors competing with the metal center for electron density, are much higher in energy and therefore are less efficient in mixing with $n_{(O)}$ and accepting electrons from a heteroatom (Figure 2-iii). Their energies and occupancies change in response to rotation in a fashion similar to $\sigma^*_{(CM)}$ but never reach the levels comparable to or below the energies of $\sigma^*_{(CM)}$ (Figure 2-v).

(C) With the increase of metal's oxidation state, the energy of $\sigma^*_{(CM)}$ lowers and becomes more available for delocalization. This feature is further augmented by the inductive effect responsible for this phenomenon and can be inferred from the analysis of the changes in dipole moment depicted in Table 4.

(D) Moving down the group from a lighter to a heavier metal, the stabilization due to $n_{(O)} \rightarrow \sigma^*_{(CM)}$ delocalization in the *axial* complexes increases due to a more efficient orbital overlap and lowering of $\sigma^*_{(CM)}$. Conversely, the energies of the same delocalization indicator in the *equatorial* decrease moving down the group, therefore these reinforcing effects result in high axial preferences.

Minimization of dipole−dipole repulsive interactions was cited as one of the dominant factors responsible for the increased stability of axial glycosides[11] and becomes an important component leading to the origin of the α-effect.[72,73] Analysis of the calculated dipole moments does not allow for definitive conclusions regarding the impact of this feature on the stability of conformers and each case needs to be considered individually (Table 4). Reduction of dipole interactions can contribute to increased stability of selected complexes (e.g., NiCl(PMe₃)₂) but cannot be concluded as the dominant factor overriding the delocalization components. Although in certain cases dipole minimization can lead to an increase in stability of the antiperiplanar isomers (e.g., Ni or CuCl), unfavorable change

of the overall dipole moment in the synclinal isomer does not override the $n_{(O)} \rightarrow \sigma^*_{(CM)}$ delocalization. Even in cases where the dipole minimization contributes to stabilization of the synclinal isomer, the conformer with the lowest dipole moment does not necessarily overlap with the optimized synclinal structure (Figure 2-vi). In qualitative terms, the conformational energy profile does not follow the same pattern (Figure 2-i) as the dipole change depicted in Figure 2-vi. In the case of gold complexes, dipole moments of the synclinal and antiperiplanar isomers are indeed very similar, yet this case represents a unique situation. Although the analysis presented here refers to gas phase conformers, reoptimization of Cu, Ag, and Au structures in nonpolar (benzene) and polar (DMSO) solvents reveals the same preferences as shown in Figure 2-i, further supporting the notion that the dipole moment may be an important component for some structures but its role is likely supplementary in stabilizing the axial/synclinal conformers. We note that polar solvents such as DMSO tend to increase preferences toward equatorial/antiperiplanar stereoisomers (for details, see the SI).

N-Heterocyclic carbenes represent a unique class of ligands because of their superior σ-donating abilities[74] that dominate delocalization into $\sigma^*_{(CM)}$ and influence the conformational preferences. The extent of NHC σ-bond donation into $\sigma^*_{(CM)}$ quantified for Cu, Ag, and Cu complexes (entries 8, 14, and 16, Table 4) shows large E_2 values for both synclinal (24.8−183.5 kcal·mol⁻¹) and antiperiplanar (23.7−194.8 kcal·mol⁻¹) conformers leaving little room for delocalization of $n_{(O)}$ electrons. Because $n_{(O)}$ orbitals in this scenario are a weaker donor (E_2 values for $n_{(O)} \rightarrow \sigma^*_{(CM)}$ range from 5.7 to 9.3 kcal·mol⁻¹ and approximately 0.5 kcal·mol⁻¹ in synclinal and antiperiplanar structures, respectively), sterics becomes the dominant factor favoring equatorial/antiperiplanar conformers. We note that Cu−NHC complexes of tetrahydropyran are almost equienergetic and Ag/Au structures show strong preference for the axial anomer, whereas in the acyclic form, the antiperiplanar conformers are preferred for all metals. It is becoming apparent from these studies that when a competent/suitable donor is located at the apical position or in a linear configuration, the metallo-anomeric stabilization is less efficient due to a suboptimal mixing of the donor $n_{(O)}$ orbitals typically higher in energy than competing σ-donors such as the NHCs. However, if the NHC or phosphines are removed from a linear overlap, then the metallo-anomeric stabilization can be restored.

The presented findings reveal several features guiding the understanding of stereochemical outcomes of transition metal-catalyzed reactions with vicinal heteroatom substituents. A predictive nature of this model allows for design of chemical reactions that can be controlled by the anomeric/metallo-anomeric effect. For example, C1-alkaline metal complexes show strong thermodynamic equatorial preference, yet transmetalation to Zn can result in a reversal of selectivity even under thermodynamic conditions opening a possibility for cis- and trans-selective reactions from a common substrate. The thermodynamic nature of the metallo-anomeric effect indicates that incorporation of protective groups in either axial or equatorial configuration located around the carbohydrate ring and equipped with suitable coordinating atoms can modify the anomeric preferences. This hypothesis is based on the notion that C−M anomerization is a reversible process, and the propensity of the C1-transition metal complexes to undergo homolytic cleavage can be modified by a ligand.[75] While the thermodynamic properties represent only a partial picture in a catalytic system, the metallo-anomeric effect can reinforce the

kinetic anomeric effect that dictates strong axial selectivities observed in C−C and C−S cross-coupling reactions.[75] These preferences would be increased in reactions where inherently high axial selectivities are observed such as galactose or mannose. Modulation of the metal oxidation states provides an alternative route to steer the outcome toward the axial products.[66]

CONCLUSIONS

This study demonstrates that in several ways stereochemical preferences of transition metal complexes resemble the behavior of powerful acceptors such as electronegative elements. The heteroatom donors strongly interact with vicinal metal centers effectively leading to an axial orientation in cyclic systems and synclinal geometry in acyclic structures. These features are dominated by stereoelectronic effects and remain operational across a broad range of organometallic systems from groups 10, 11, and 12 due to efficient mixing of nonbonding electrons with low-lying C−M antibonding orbitals. While the classical anomeric effect has been harnessed to develop chemical glycosylations and organocatalytic transformations,[76] utilization of analogous stereoelectronic interactions in modern transition metal-catalyzed reactions remains virtually unexplored.[77] By regulating the steric and electronic properties of ligands, metal oxidation states and geometry, new avenues for reaction development become available.

ASSOCIATED CONTENT

Ⓢ Supporting Information

The Supporting Information is available free of charge at https://pubs.acs.org/doi/10.1021/jacs.0c06882.

> Computational details and Cartesian coordinates for all structures (PDF)

AUTHOR INFORMATION

Corresponding Author

Maciej A. Walczak − *Department of Chemistry, University of Colorado, Boulder, Colorado 80309, United States;* ⓞ orcid.org/0000-0002-8049-0817; Email: maciej.walczak@colorado.edu

Author

Feng Zhu − *Department of Chemistry, University of Colorado, Boulder, Colorado 80309, United States*

Complete contact information is available at: https://pubs.acs.org/10.1021/jacs.0c06882

Notes

The authors declare no competing financial interest.

ACKNOWLEDGMENTS

REFERENCES

(1) Deslongchamps, P. *Stereoelectronic Effects in Organic Chemistry*; Pergamon Press: Exeter, 1983.

(2) Alabugin, I. V. *Stereoelectronic Effects: A Bridge Between Structure and Reactivity*; John Wiley & Sons, Ltd.: New York, 2016.

(3) Eliel, E. L.; Giza, C. A. Conformational analysis. XVII. 2-Alkoxy- and 2-alkylthiotetrahydropyrans and 2-alkoxy-1,3-dioxanes. Anomeric effect. *J. Org. Chem.* **1968**, *33*, 3754−3758.

(4) Lemieux, R. U. Effects of unshared pairs of electrons and their solvation on conformational equilibria. *Pure Appl. Chem.* **1971**, *25*, 527.

(5) Kirby, A. J. *The Anomeric Effect and Related Stereoelectronic Effects at Oxygen*; Springer: New York, 1983.

(6) Box, V. G. S. The Role of Lone Pair Interactions in the Chemistry of the Monosaccharides. The Anomeric Effects. *Heterocycles* **1990**, *31*, 1157−1181.

(7) Juaristi, E.; Cuevas, G. Recent studies of the anomeric effect. *Tetrahedron* **1992**, *48*, 5019−5087.

(8) Thatcher, G. R. J. *The Anomeric Effect and Associated Stereoelectronic Effects.* ACS: Washington, DC, 1993.

(9) Salzner, U.; Schleyer, P. v. R. Ab Initio Examination of Anomeric Effects in Tetrahydropyrans, 1,3-Dioxanes, and Glucose. *J. Org. Chem.* **1994**, *59*, 2138−2155.

(10) Cocinero, E. J.; Carcabal, P.; Vaden, T. D.; Simons, J. P.; Davis, B. G. Sensing the anomeric effect in a solvent-free environment. *Nature* **2011**, *469*, 76−79.

(11) Mo, Y. Computational evidence that hyperconjugative interactions are not responsible for the anomeric effect. *Nat. Chem.* **2010**, *2*, 666.

(12) Cramer, C. J.; Truhlar, D. G.; French, A. D. Exo-anomeric effects on energies and geometries of different conformations of glucose and related systems in the gas phase and aqueous solution. *Carbohydr. Res.* **1997**, *298*, 1−14.

(13) Lemieux, R. U.; Morgan, A. R. The Abnormal Conformations of Pyridinium α-Glycopyranosides. *Can. J. Chem.* **1965**, *43*, 2205−2213.

(14) Perrin, C. L. Reverse anomeric effect: fact or fiction? *Tetrahedron* **1995**, *51*, 11901−11935.

(15) Wolfe, S. Gauche effect. Stereochemical consequences of adjacent electron pairs and polar bonds. *Acc. Chem. Res.* **1972**, *5*, 102−111.

(16) Wiberg, K. B.; Murcko, M. A. Rotational barriers. 4. Dimethoxymethane. The anomeric effect revisited. *J. Am. Chem. Soc.* **1989**, *111*, 4821−4828.

(17) Vila, A.; Mosquera, R. A. Atoms in molecules interpretation of the anomeric effect in the O−C−O unit. *J. Comput. Chem.* **2007**, *28*, 1516−1530.

(18) Nicolas, L.; Angibaud, P.; Stansfield, I.; Bonnet, P.; Meerpoel, L.; Reymond, S.; Cossy, J. Diastereoselective Metal-Catalyzed Synthesis of C-Aryl and C-Vinyl Glycosides. *Angew. Chem., Int. Ed.* **2012**, *51*, 11101−11104.

(19) Gong, H.; Gagne, M. R. Diastereoselective Ni-catalyzed Negishi cross-coupling approach to saturated, fully oxygenated C-alkyl and C-aryl glycosides. *J. Am. Chem. Soc.* **2008**, *130*, 12177.

(20) Gong, H.; Andrews, R. S.; Zuccarello, J. L.; Lee, S. J.; Gagné, M. R. Sn-Free Ni-Catalyzed Reductive Coupling of Glycosyl Bromides with Activated Alkenes. *Org. Lett.* **2009**, *11*, 879−882.

(21) Zhao, C.; Jia, X.; Wang, X.; Gong, H. Ni-Catalyzed Reductive Coupling of Alkyl Acids with Unactivated Tertiary Alkyl and Glycosyl Halides. *J. Am. Chem. Soc.* **2014**, *136*, 17645−17651.

(22) Liu, J.; Gong, H. Stereoselective Preparation of α-C-Vinyl/Aryl Glycosides via Nickel-Catalyzed Reductive Coupling of Glycosyl Halides with Vinyl and Aryl Halides. *Org. Lett.* **2018**, *20*, 7991−7995.

(23) Badir, S. O.; Dumoulin, A.; Matsui, J. K.; Molander, G. A. Synthesis of Reversed C-Acyl Glycosides through Ni/Photoredox Dual Catalysis. *Angew. Chem., Int. Ed.* **2018**, *57*, 6610−6613.

(24) Dumoulin, A.; Matsui, J. K.; Gutiérrez-Bonet, Á.; Molander, G. A. Synthesis of Non-Classical Arylated C-Saccharides through Nickel/Photoredox Dual Catalysis. *Angew. Chem., Int. Ed.* **2018**, *57*, 6614−6618.

(25) Adak, L.; Kawamura, S.; Toma, G.; Takenaka, T.; Isozaki, K.; Takaya, H.; Orita, A.; Li, H. C.; Shing, T. K. M.; Nakamura, M. Synthesis of Aryl C-Glycosides via Iron-Catalyzed Cross Coupling of

Halosugars: Stereoselective Anomeric Arylation of Glycosyl Radicals. *J. Am. Chem. Soc.* **2017**, *139*, 10693−10701.

(26) Coote, M. L.; Lin, C. Y.; Beckwith, A. L.; Zavitsas, A. A. A comparison of methods for measuring relative radical stabilities of carbon-centred radicals. *Phys. Chem. Chem. Phys.* **2010**, *12*, 9597−9610.

(27) Poutsma, M. L. The radical stabilization energy of a substituted carbon-centered free radical depends on both the functionality of the substituent and the ordinality of the radical. *J. Org. Chem.* **2011**, *76*, 270−276.

(28) Amani, J.; Sodagar, E.; Molander, G. A. Visible light photoredox cross-coupling of acyl chlorides with potassium alkoxymethyltrifluoroborates: synthesis of α-alkoxyketones. *Org. Lett.* **2016**, *18*, 732−735.

(29) Karimi-Nami, R.; Tellis, J. C.; Molander, G. A. Single-electron transmetalation: protecting-group-independent synthesis of secondary benzylic alcohol derivatives via photoredox/nickel dual catalysis. *Org. Lett.* **2016**, *18*, 2572−2575.

(30) El Khatib, M.; Serafim, R. A. M.; Molander, G. A. α-Arylation/ Heteroarylation of Chiral α-Aminomethyltrifluoroborates by Synergistic Iridium Photoredox/Nickel Cross-Coupling Catalysis. *Angew. Chem., Int. Ed.* **2016**, *55*, 254−258.

(31) Amani, J.; Alam, R.; Badir, S.; Molander, G. A. Synergistic Visible-Light Photoredox/Nickel-Catalyzed Synthesis of Aliphatic Ketones via N−C Cleavage of Imides. *Org. Lett.* **2017**, *19*, 2426−2429.

(32) Amani, J.; Molander, G. A. Direct conversion of carboxylic acids to alkyl ketones. *Org. Lett.* **2017**, *19*, 3612−3615.

(33) Matsui, J. K.; Molander, G. A. Direct α-arylation/heteroarylation of 2-trifluoroboratochromanones via photoredox/nickel dual catalysis. *Org. Lett.* **2017**, *19*, 436−439.

(34) Alam, R.; Molander, G. A. Direct synthesis of secondary benzylic alcohols enabled by photoredox/Ni dual-catalyzed cross-coupling. *J. Org. Chem.* **2017**, *82*, 13728−13734.

(35) Corcé, V.; Chamoreau, L. M.; Derat, E.; Goddard, J. P.; Ollivier, C.; Fensterbank, L. Silicates as Latent Alkyl Radical Precursors: Visible-Light Photocatalytic Oxidation of Hypervalent Bis-Catecholato Silicon Compounds. *Angew. Chem., Int. Ed.* **2015**, *54*, 11414−11418.

(36) Lévêque, C.; Chenneberg, L.; Corcé, V.; Goddard, J.-P.; Ollivier, C.; Fensterbank, L. Primary alkyl bis-catecholato silicates in dual photoredox/nickel catalysis: aryl-and heteroaryl-alkyl cross coupling reactions. *Org. Chem. Front.* **2016**, *3*, 462−465.

(37) Remeur, C.; Kelly, C. B.; Patel, N. R.; Molander, G. A. Aminomethylation of aryl halides using α-silylamines enabled by Ni/ photoredox dual catalysis. *ACS Catal.* **2017**, *7*, 6065−6069.

(38) Noble, A.; McCarver, S. J.; MacMillan, D. W. C. Merging Photoredox and Nickel Catalysis: Decarboxylative Cross-Coupling of Carboxylic Acids with Vinyl Halides. *J. Am. Chem. Soc.* **2015**, *137*, 624−627.

(39) Zuo, Z.; Cong, H.; Li, W.; Choi, J.; Fu, G. C.; MacMillan, D. W. Enantioselective decarboxylative arylation of α-amino acids via the merger of photoredox and nickel catalysis. *J. Am. Chem. Soc.* **2016**, *138*, 1832−1835.

(40) Johnston, C. P.; Smith, R. T.; Allmendinger, S.; MacMillan, D. W. Metallaphotoredox-catalysed sp 3−sp 3 cross-coupling of carboxylic acids with alkyl halides. *Nature* **2016**, *536*, 322−325.

(41) Till, N. A.; Smith, R. T.; MacMillan, D. W. C. Decarboxylative Hydroalkylation of Alkynes. *J. Am. Chem. Soc.* **2018**, *140*, 5701−5705.

(42) Shea, M. D.; Mansoor, U. F.; Hopkins, B. A. A Metallaphotoredox Method for the Expansion of Benzyl SAR on Electron-Deficient Amines. *Org. Lett.* **2020**, *22*, 1052−1055.

(43) Yue, H.; Zhu, C.; Kancherla, R.; Liu, F.; Rueping, M. Regioselective Hydroalkylation and Arylalkylation of Alkynes by Photoredox/Nickel Dual Catalysis: Application and Mechanism. *Angew. Chem., Int. Ed.* **2020**, *59*, 5738−5746.

(44) Gutierrez-Bonet, A.; Tellis, J. C.; Matsui, J. K.; Vara, B. A.; Molander, G. A. 1,4-Dihydropyridines as alkyl radical precursors: introducing the aldehyde feedstock to nickel/photoredox dual catalysis. *ACS Catal.* **2016**, *6*, 8004−8008.

(45) Zhang, P.; Le, C. C.; MacMillan, D. W. Silyl radical activation of alkyl halides in metallaphotoredox catalysis: a unique pathway for cross-electrophile coupling. *J. Am. Chem. Soc.* **2016**, *138*, 8084−8087.

(46) Shaw, M. H.; Shurtleff, V. W.; Terrett, J. A.; Cuthbertson, J. D.; MacMillan, D. W. Native functionality in triple catalytic cross-coupling: sp3 C−H bonds as latent nucleophiles. *Science* **2016**, *352*, 1304−1308.

(47) Heitz, D. R.; Tellis, J. C.; Molander, G. A. Photochemical nickel-catalyzed C−H arylation: synthetic scope and mechanistic investigations. *J. Am. Chem. Soc.* **2016**, *138*, 12715−12718.

(48) Ahneman, D. T.; Doyle, A. G. C−H functionalization of amines with aryl halides by nickel-photoredox catalysis. *Chem. Sci.* **2016**, *7*, 7002−7006.

(49) Shields, B. J.; Doyle, A. G. Direct C (sp3)−H cross coupling enabled by catalytic generation of chlorine radicals. *J. Am. Chem. Soc.* **2016**, *138*, 12719−12722.

(50) Le, C.; Liang, Y.; Evans, R. W.; Li, X.; MacMillan, D. W. Selective sp 3 C−H alkylation via polarity-match-based cross-coupling. *Nature* **2017**, *547*, 79−83.

(51) Deng, H.-P.; Fan, X.-Z.; Chen, Z.-H.; Xu, Q.-H.; Wu, J. Photoinduced nickel-catalyzed chemo-and regioselective hydroalkylation of internal alkynes with ether and amide α-hetero C (sp3)−H bonds. *J. Am. Chem. Soc.* **2017**, *139*, 13579−13584.

(52) Nielsen, M. K.; Shields, B. J.; Liu, J.; Williams, M. J.; Zacuto, M. J.; Doyle, A. G. Mild, Redox-Neutral Formylation of Aryl Chlorides through the Photocatalytic Generation of Chlorine Radicals. *Angew. Chem., Int. Ed.* **2017**, *56*, 7191−7194.

(53) Twilton, J.; Christensen, M.; DiRocco, D. A.; Ruck, R. T.; Davies, I. W.; MacMillan, D. W. Selective Hydrogen Atom Abstraction through Induced Bond Polarization: Direct α-Arylation of Alcohols through Photoredox, HAT, and Nickel. *Angew. Chem., Int. Ed.* **2018**, *57*, 5369−5373.

(54) Ackerman, L. K.; Martinez Alvarado, J. I.; Doyle, A. G. Direct C−C bond formation from alkanes using Ni-photoredox catalysis. *J. Am. Chem. Soc.* **2018**, *140*, 14059−14063.

(55) Murarka, S. N-(Acyloxy) phthalimides as Redox-Active Esters in Cross-Coupling Reactions. *Adv. Synth. Catal.* **2018**, *360*, 1735−1753.

(56) Toriyama, F.; Cornella, J.; Wimmer, L.; Chen, T.-G.; Dixon, D. D.; Creech, G.; Baran, P. S. Redox-active esters in Fe-catalyzed C−C coupling. *J. Am. Chem. Soc.* **2016**, *138*, 11132−11135.

(57) Cornella, J.; Edwards, J. T.; Qin, T.; Kawamura, S.; Wang, J.; Pan, C.-M.; Gianatassio, R.; Schmidt, M.; Eastgate, M. D.; Baran, P. S. Practical Ni-catalyzed aryl−alkyl cross-coupling of secondary redox-active esters. *J. Am. Chem. Soc.* **2016**, *138*, 2174−2177.

(58) Wang, J.; Qin, T.; Chen, T. G.; Wimmer, L.; Edwards, J. T.; Cornella, J.; Vokits, B.; Shaw, S. A.; Baran, P. S. Nickel-catalyzed cross-coupling of redox-active esters with boronic acids. *Angew. Chem., Int. Ed.* **2016**, *55*, 9676−9679.

(59) Qin, T.; Cornella, J.; Li, C.; Malins, L. R.; Edwards, J. T.; Kawamura, S.; Maxwell, B. D.; Eastgate, M. D.; Baran, P. S. A general alkyl-alkyl cross-coupling enabled by redox-active esters and alkylzinc reagents. *Science* **2016**, *352*, 801−805.

(60) Li, C.; Wang, J.; Barton, L. M.; Yu, S.; Tian, M.; Peters, D. S.; Kumar, M.; Yu, A. W.; Johnson, K. A.; Chatterjee, A. K.; Yan, M.; Baran, P. S. Decarboxylative borylation. *Science* **2017**, *356*, eaam7355.

(61) Wang, J.; Shang, M.; Lundberg, H.; Feu, K. S.; Hecker, S. J.; Qin, T.; Blackmond, D. G.; Baran, P. S. Cu-catalyzed decarboxylative borylation. *ACS Catal.* **2018**, *8*, 9537−9542.

(62) Wittmann, V.; Kessler, H. Stereoselective Synthesis of C-Glycoside with a Glycosyl Dianion. *Angew. Chem., Int. Ed. Engl.* **1993**, *32*, 1091−1093.

(63) Zhu, F.; Rodriguez, J.; Yang, T.; Kevlishvili, I.; Miller, E.; Yi, D.; O'Neill, S.; Rourke, M. J.; Liu, P.; Walczak, M. A. Glycosyl Cross-Coupling of Anomeric Nucleophiles: Scope, Mechanism, and Applications in the Synthesis of Aryl C-Glycosides. *J. Am. Chem. Soc.* **2017**, *139*, 17908−17922.

(64) Hoang, K. M.; Lees, N. R.; Herzon, S. B. Programmable Synthesis of 2-Deoxyglycosides. *J. Am. Chem. Soc.* **2019**, *141*, 8098−8103.

(65) Eliel, E. L.; Wilen, S. H.; Mander, L. N. *Stereochemistry of Organic Compounds*; Wiley: New York, 1994.

(66) Wang, Q.; An, S.; Deng, Z.; Zhu, W.; Huang, Z.; He, G.; Chen, G. Palladium-catalysed C−H glycosylation for synthesis of C-aryl glycosides. *Nat. Catal.* **2019**, *2*, 793−800.

(67) Alabugin, I. V.; Zeidan, T. A. Stereoelectronic Effects and General Trends in Hyperconjugative Acceptor Ability of σ Bonds. *J. Am. Chem. Soc.* **2002**, *124*, 3175−3185.

(68) Juaristi, E. Conformational analysis of six-membered, sulfur-containing saturated heterocycles. *Acc. Chem. Res.* **1989**, *22*, 357−364.

(69) Gomes, G. d. P.; Vil, V.; Terent'ev, A.; Alabugin, I. V. Stereoelectronic source of the anomalous stability of bis-peroxides. *Chem. Sci.* **2015**, *6*, 6783−6791.

(70) Reed, A. E.; Curtiss, L. A.; Weinhold, F. Intermolecular interactions from a natural bond orbital, donor-acceptor viewpoint. *Chem. Rev.* **1988**, *88*, 899−926.

(71) Freitas, M. P. The anomeric effect on the basis of natural bond orbital analysis. *Org. Biomol. Chem.* **2013**, *11*, 2885−2890.

(72) Buncel, E.; Um, I.-H. The α-effect and its modulation by solvent. *Tetrahedron* **2004**, *60*, 7801−7825.

(73) Juaristi, E.; dos Passos Gomes, G.; Terent'ev, A. O.; Notario, R.; Alabugin, I. V. Stereoelectronic Interactions as a Probe for the Existence of the Intramolecular α-Effect. *J. Am. Chem. Soc.* **2017**, *139*, 10799−10813.

(74) Bourissou, D.; Guerret, O.; Gabbaï, F. P.; Bertrand, G. Stable Carbenes. *Chem. Rev.* **2000**, *100*, 39−92.

(75) Zhu, F.; Zhang, S.-q.; Chen, Z.; Rui, J.; Hong, X.; Walczak, M. A. Catalytic and Photochemical Strategies to Stabilized Radicals Based on Anomeric Nucleophiles. *J. Am. Chem. Soc.* **2020**, *142*, 11102−11113.

(76) Aufiero, M.; Gilmour, R. Informing Molecular Design by Stereoelectronic Theory: The Fluorine Gauche Effect in Catalysis. *Acc. Chem. Res.* **2018**, *51*, 1701−1710.

(77) Vidhani, D. V.; Krafft, M. E.; Alabugin, I. V. Gold(I)-Catalyzed Allenyl Cope Rearrangement: Evolution from Asynchronicity to Trappable Intermediates Assisted by Stereoelectronic Switching. *J. Am. Chem. Soc.* **2016**, *138*, 2769−2779.